JOURNAL OF GEOPHYSICAL RESEARCH, VOL. 107, NO. D22, 4635, doi:10.1029/2002JD002195, 2002

On error estimation in atmospheric CO_2 inversions

Richard J. Engelen,[1] A. Scott Denning, and Kevin R. Gurney
Department of Atmospheric Science, Colorado State University, Fort Collins, Colorado, USA

TransCom3 modelers[2]

Received 11 February 2002; revised 31 May 2002; accepted 15 June 2002; published 22 November 2002.

[1] This paper explores various sources of error in atmospheric CO_2 synthesis inversions using global circulation models. The estimation of prior, observation, model transport, and representation errors is described, and the latter two error sources are explored in more detail. Not accounting for these errors will act as a hard constraint on the inversion and will produce incorrect solutions to the problem as is shown in some example inversions. The magnitude of these errors falls generally between about 10% and 100% in the retrieved fluxes but can be even larger. This makes it highly desirable to avoid hard constraints and apply any prior information we have about the surface fluxes as a weak constraint to the inversion problem. *INDEX TERMS:* 0315 Atmospheric Composition and Structure: Biosphere/atmosphere interactions; 0322 Atmospheric Composition and Structure: Constituent sources and sinks; 0330 Atmospheric Composition and Structure: Geochemical cycles; 1615 Global Change: Biogeochemical processes (4805); *KEYWORDS:* CO_2, model inversion, error, fluxes

Citation: Engelen, R. J., A. S. Denning, K. R. Gurney, and TransCom3 modelers, On error estimation in atmospheric CO_2 inversions, *J. Geophys. Res.*, *107*(D22), 4635, doi:10.1029/2002JD002195, 2002.

1. Introduction

[2] Spatial and temporal variations of atmospheric CO_2 concentration contain information about sources and sinks, which may be quantitatively interpreted using inverse modeling of tracer transport [e.g., *Tans et al.*, 1990; *Enting et al.*, 1995; *Rayner et al.*, 1999; *Gurney et al.*, 2002]. Synthesis inversion involves the forward simulation of the concentration response to unit amounts of emissions from specified regions and times, using an atmospheric tracer transport model. Linear combinations of these response functions are then combined to produce optimal agreement with measured concentrations, typically using least squares methods [e.g., *Enting*, 2002].

[3] We refer to the set of locations and times of unit emissions that are scaled by the inversion as "basis functions." The methodology adopted for the Atmospheric CO_2 Inversion Intercomparison Project (TransCom3) is typical of recent inversion studies: it sought to optimize source/sink magnitudes from 22 regions and 12 months of an average year [*Gurney et al.*, 2000]. Figure 1 shows these 22 regions with the prescribed flux patterns within two of those regions as insets.

[4] Unfortunately, the current observing network is very sparse, consisting primarily of weekly samples taken in remote marine locations, and response functions arising from emissions at the various regions and times can be used in different combinations to match the same set of observations. Given this ill-conditioning, strict optimization of the source/sink strengths in inverse models tends to produce dipoles in poorly observed regions with magnitudes that are completely unrealistic. A 12 Gt C yr^{-1} source in Africa, for example, might be paired with a 13 Gt C yr^{-1} sink in South America and produce the best agreement with observed concentrations, yet we know that such fluxes are wildly unrealistic.

[5] To avoid such pitfalls arising from weak data constraints, most inversion studies have relied on "regularization" techniques. These include truncation of the dimensions of the problem to estimate fluxes from only a few large regions or time averages [e.g., *Fan et al.*, 1998], numerical truncation using singular value decomposition [*Baker*, 2001], and the use of "prior constraints" in a Bayesian framework [e.g., *Tarantola*, 1987] to penalize solutions which produce unreasonable values [*Rayner et al.*, 1999; *Bousquet et al.*, 2000; *Gurney et al.*, 2002]. The inversion formalism commonly used propagates the uncertainty in these prior constraints through the calculation, balancing it against uncertainty in the measurements to obtain the optimized solution.

[6] A recent paper by *Kaminski et al.* [2001] (hereinafter referred to as Kam2001) demonstrated that regularizing the solution by spatial truncating (lumping) small basis regions into larger combined ones introduces error. This "aggregation error" was shown to arise because the observed and simulated concentration field may be sensitive to the spatial distribution of sources and sinks within large regions, but the inversion is not free to adjust these subregional patterns. Unlike the Bayesian priors, subregional patterns are typi-

[1] Now at ECMWF, Shinfield Park, Reading, UK.

[2] K. R. Gurney, R. M. Law, A. S. Denning, P. J. Rayner, D. Baker, P. Bousquet, L. Bruhwiler, Y.-H. Chen, P. Ciais, S. Fan, I. Y. Fung, M. Gloor, M. Heimann, K. Higuchi, J. John, T. Maki, S. Maksyutov, K. Masarie, P. Peylin, M. Prather, B. C. Pak, J. Sarmiento, S. Taguchi, T. Takahashi, and C.-W. Yuen.

0148-0227/02/2002JD002195$09.00

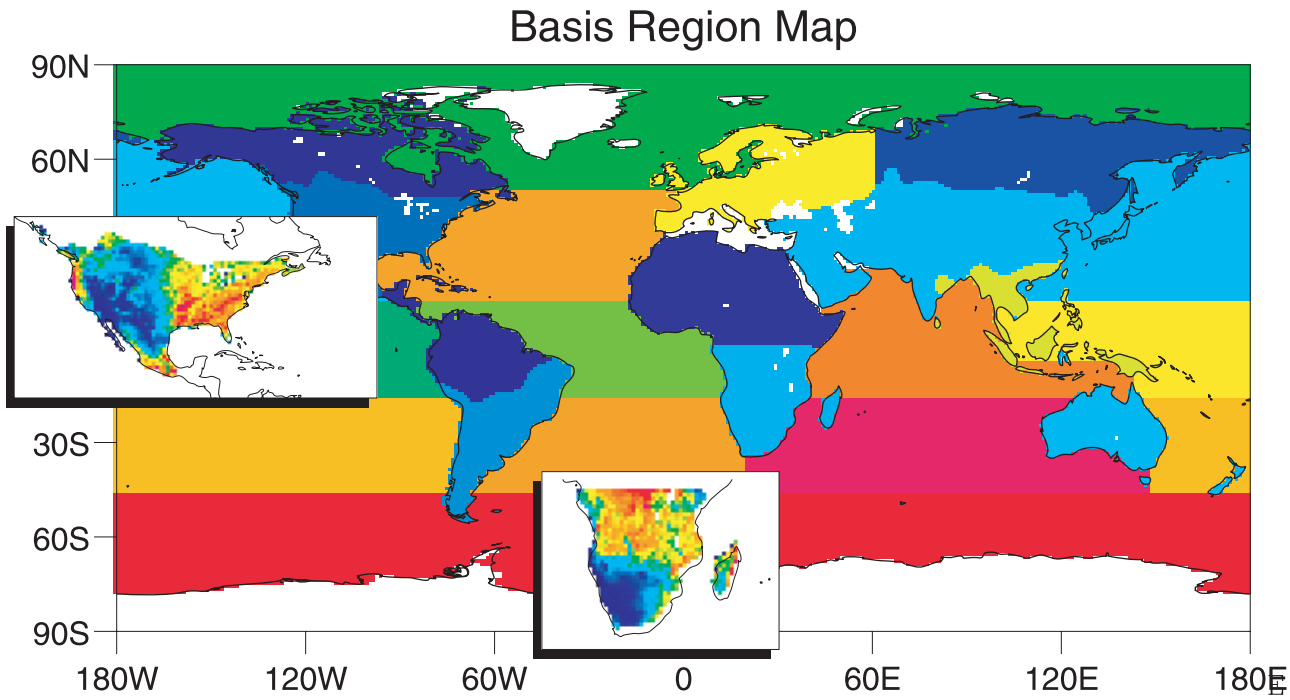

Figure 1. Map of the 22 basis regions used in the TransCom3 experiment. The two inserts show the basis functions on a 0.5° × 0.5° grid for the Temperate North American and the South African basis regions.

cally prescribed in inversions as a "hard constraint." Errors in these patterns cannot be corrected by the inversion procedure, and the resulting error is unavoidably aliased into the resolved sources and sinks. This is not a problem if the pattern of fluxes is correctly known a priori, but in general these patterns cannot be evaluated. To avoid introducing bias in optimized fluxes, Kam2001 recommend using an algorithm that calculates the impact of these errors on the simulated observations used in the inversion. This allows, according to Kam2001, proper accounting for these errors. We will show later that is only partly true. General discussions about the use of hard and weak constraints in inversion problems are given by *Wunsch* [1996] and *Rodgers* [2000].

[7] There are a number of other hard constraints used in most inversion studies, besides the subregional spatial distribution of fluxes associated with each basis function. The temporal phasing of the fluxes (seasonal and diurnal cycles, for example) is often specified and cannot be adjusted by the inversion [*Fan et al.*, 1998]. The simulated transport in a given model introduces unavoidable error and similarly cannot be adjusted. Fluxes due to "background" processes such as fossil fuel combustion, air–sea gas exchanges, and purely seasonal exchange with the terrestrial biosphere (rectifier effects) are similarly often prescribed as hard constraints in recent inversions [*Gurney et al.*, 2002]. In each of these cases, error in the specified hard constraints is unavoidably aliased into the resolved fluxes.

[8] In this paper we explore the various sources of error present in CO_2 inversions, and estimate their magnitudes. We investigate the effects of each of the hard constraints on the optimized fluxes and their errors. In section 2, we present the theoretical framework and define several sources of error. In section 3, we consider the effects of transport error, and in section 4 we explore the impact of representation errors. Finally, in section 5 we present conclusions.

2. Inversion Theory and Error Sources

2.1. General

[9] To estimate surface fluxes $\mathbf{s}$ from observational data $\mathbf{d}$, given a prior estimate of the surface fluxes $\mathbf{s}_0$, we minimize the following cost function:

$$\Phi = [\mathbf{Gs} - \mathbf{d}]^T \mathbf{C}(\mathbf{d})^{-1} [\mathbf{Gs} - \mathbf{d}] + [\mathbf{s} - \mathbf{s}_0]^T \mathbf{C}(\mathbf{s}_0)^{-1} [\mathbf{s} - \mathbf{s}_0] \quad (1)$$

where $\mathbf{G}$ is the Jacobian of the transport model, which maps the surface fluxes to the data and which is often referred to as the response functions of the transport model, and $\mathbf{C}(\mathbf{s}_0)$ is the prior covariance matrix that describes the uncertainty in our prior estimate of the surface fluxes. $\mathbf{C}(\mathbf{d})$ is the covariance matrix describing the expected difference between the observational data and the model simulations, which includes several error sources besides the observation error:

$$\mathbf{C}(\mathbf{d}) = \mathbf{O} + \mathbf{M} + \mathbf{T} + \mathbf{F} \quad (2)$$

where $\mathbf{O}$ is the observation error covariance describing the errors in the observations (calibration, etc.), $\mathbf{M}$ is the mapping error covariance describing the errors in mapping CO_2 concentrations at a specific location into the measured quantity (e.g., satellite radiances), $\mathbf{T}$ is the model transport error covariance describing the errors in mapping the fluxes into CO_2 concentrations at the various observational sites,

and **F** is the representation error covariance describing the effects of model resolution. Minimizing the cost function in equation (1) provides the following solution:

$$\hat{\mathbf{s}} = \left[\mathbf{G}^T\mathbf{C}(\mathbf{d})^{-1}\mathbf{G} + \mathbf{C}(\mathbf{s}_0)^{-1}\right]^{-1}\left[\mathbf{G}^T\mathbf{C}(\mathbf{d})^{-1}\mathbf{d} + \mathbf{C}(\mathbf{s}_0)^{-1}\mathbf{s}_0\right] \quad (3)$$

Because the solution ($\hat{\mathbf{s}}$) in our Bayesian setup is a weighted average of the prior estimate and the observations weighted by the respective covariance matrices, it is crucial to have a good understanding of the errors represented by the covariance matrices in order to obtain the most optimal solution. Using inaccurate covariance matrices can lead to nonoptimal solutions or in some cases even to spurious solutions due to mathematical oscillations in the solution. In the following subsections we will discuss each of the error covariance matrices in more detail. The assumptions we will make are that the errors contain no biases and that the four error sources forming $\mathbf{C}(\mathbf{d})$ are uncorrelated. The latter assumption, however, is not strictly valid, because both the model transport error and the representation error depend on the surface flux distribution as will be shown in the next sections. The assumption, therefore, is that the cross correlations between these error sources are much smaller than the individual error covariances describing these error sources. The validation of this assumption is beyond the scope of this paper and will be subject of further study.

2.2. Prior Error

[10] Prior constraint on source strengths is needed to avoid unrealistic solutions that arise because of poor data coverage over much of the world and the ill-conditioned nature of the inversion problem. These prior constraints include both the global mass balance of atmospheric CO_2 (known very accurately from the flask record) and estimates of fluxes from each of the regions and months for which fluxes are sought (generally known only poorly). These variable uncertainties are expressed by the prior source covariance matrix ($\mathbf{C}(\mathbf{s}_0)$). Typical recent inversion calculations have used zero as a prior source estimate for each basis region, with or without a ''background'' or presubtracted field derived from some combination of direct measurement, models, or satellite observations. In the TransCom3 experiment, background fluxes due to fossil fuel emissions (from economic data) [*Andres et al.*, 1996], seasonal exchange with a balanced terrestrial biosphere (using a model driven by observed climate and satellite vegetation data) [*Randerson et al.*, 1997], and air–sea fluxes (interpolated from millions of in situ measurements) [*Takahashi et al.*, 1999] were prescribed a priori. Prior uncertainty in each of these presubtracted fields was assumed to be very small, partly because the fluxes are known rather well relative to other parts of the problem, and partly because corrections to these fields are made in each of the 22 basis regions. Also, neither the neutral biosphere nor the air–sea flux is positive definite, changing signs both over the spatial domain and at given locations through the year. Thus it is not appropriate to simply scale them in the inversion since substantial cancellation would result. Prior estimates of regional fluxes are typically set to zero, with generous prior error estimates to allow the solution to be data driven but still prevent spurious dipoles. For annual mean inversions in the TransCom3 experiment, most regions were assumed to have zero fluxes, but some land use information was also applied [*Gurney et al.*, 2002]. Prior uncertainty estimates in the oceans were set according to the density of observations used to construct the background flux field [*Takahashi et al.*, 1999]. Prior uncertainty on land was set equal to the growing season net flux (sum of all monthly background fluxes during the period when the region is a net sink).

2.3. Observation and Mapping Error

[11] The observation error (**O**) is in general easily quantifiable by careful calibration of the instruments. Correlations between measurement errors are usually set to zero, allowing the use of a diagonal matrix for the covariance matrix. Analytical error in CO_2 mole fraction is assessed by calibration and analysis of samples of known quantity in blind tests. This source of error is small, generally within 0.05 ppmv [*Masarie et al.*, 2001]. Other important sources of direct observation error are introduced by sample collection processing equipment, and by the fact that interlaboratory calibrations across the network are difficult to maintain. The latter source of error is likely the most significant, and is regularly assessed by round robin comparisons of analyses of common flask samples by multiple laboratories. Interlaboratory differences are believed to contribute at least 0.2 ppmv uncertainty in measured mole fraction [*World Meteorological Organisation* (*WMO*), 1995, 1999].

[12] When we include any remote observations of CO_2 in the inversion, we need to include the mapping error covariance **M**. It describes the error caused by retrieving a CO_2 concentration from an indirect observation (e.g., satellite observed radiances). In its simplest form it is just the retrieved CO_2 uncertainty, comparable to the observation error covariance **O**. However, if the indirect observations are used directly in the inversion, this covariance matrix describes the errors in the mapping operator (e.g., a forward radiative transfer model). The first form would come directly from a CO_2 retrieval algorithm, the second form would have to be estimated by comparing the used mapping operator to similar or better mapping operators (e.g., a fast radiative transfer model could be compared to a line-by-line radiative transfer model). A possibly serious error arises when the observation errors are correlated in space and/or time. For instance, satellite observations could be dependent on the surface albedo. If we do not know this surface albedo accurately, the retrieved CO_2 concentrations over land could be biased with respect to the retrieved CO_2 concentrations over ocean. These regional biases can introduce error in the retrieved fluxes, since they create nonexistent spatial gradients. It is therefore crucial to be aware of any biases in the observations.

2.4. Transport Error

[13] The transport error (**T**) is a very important contributor to the overall error budget of CO_2 inversions, whose importance is likely to be amplified as additional observations become available [*Denning et al.*, 2001]. It can be split up into two components: the transport model error and the transport model parameter error. The first error represents any simplification of the real physics and dynamics in the

transport model (e.g., convective parameterizations) and is defined as

$$\Delta G \equiv g(\mathbf{s}, \mathbf{b}, \mathbf{b}') - G(\mathbf{s}, \mathbf{b}) \quad (4)$$

where $g(\mathbf{s}, \mathbf{b})$ represents the real world dynamics and G the model formulation. The real surface fluxes are denoted by $\mathbf{s}$ and all other variables that influence the CO_2 concentrations at the observation sites are denoted by $\mathbf{b}$ and $\mathbf{b}'$ (e.g., horizontal winds, vertical diffusion). The difference between $\mathbf{b}$ and $\mathbf{b}'$ is that $\mathbf{b}$ consists of variables that are actually modeled, while $\mathbf{b}'$ are the variables that are ignored in the transport model. ΔG therefore represents the error in the simulated observations that is made by using simplified physics to model the real world. As noted earlier it depends on the surface flux distribution. This transport model error tends to be systematic and is generally hard to estimate, since we can not exactly model the real world dynamics and physics (g). However, comparisons with high resolution transport models (e.g., numerical weather forecast models) can give an estimate of this bias.

[14] The second error (transport model parameter error) represents the effect of errors on any model parameter and is defined as

$$\mathbf{T} = \mathbf{K}_b \mathbf{C}(\mathbf{b}) \mathbf{K}_b^T \quad (5)$$

where $\mathbf{K} = \partial G / \partial \mathbf{b}$ and $\mathbf{C}(\mathbf{b}) = \varepsilon\{(\hat{\mathbf{b}} - \mathbf{b})(\hat{\mathbf{b}} - \mathbf{b})^T\}$, where ε is the expectation operator and $\hat{\mathbf{b}}$ is our estimate of the variables $\mathbf{b}$. A first attempt to estimate this error will be described in section 3.

2.5. Representation Error

[15] We define two types of representation error involved in CO_2 inversions, the internal and external representation error. The internal representation error describes the errors that arise when we perform the CO_2 model inversion on a different grid (both space and time) than the transport model grid. This inversion grid can be just an aggregation of grid boxes, but is more commonly a representation of the surface fluxes on large basis regions [e.g., *Gurney et al.*, 2002]. The error represents the mismatch in resolution between the forward model calculations to obtain the transport operator $\mathbf{G}$ (e.g., 72×44 grid boxes on 30 min time intervals) and the inversion performed on the monthly means of for instance 22 basis regions. It was this source of error that was investigated by Kam2001, and termed aggregation error. Since this is a complicated but important error source, we will describe this error source in more detail in section 4.

[16] The external representation error involves mismatches between the model simulation and the observations, in both space and time. Flask samples are taken from a continuously varying concentration field, and are influenced by many factors not present in the transport models used for typical inversions. External representation error includes spatial variations at scales smaller than the model grid boxes, and time variations at scales shorter than the sampling frequency of the observations. Many inversions optimize simulated monthly mean concentrations over areas as large as 10^5 km^2 through depths of up to 1 km against point samples taken at the surface once a week, for example. External representation error may also include unresolvable transport due to synoptic, mesoscale or local phenomena. Local- or regional-scale emissions or sinks (for example, a factory or power plant in a particular direction from a sampling site) that cannot be correctly represented in a model also lead to errors of this kind. Sampling protocols are designed to obtain background air that is representative of large upstream regions and as free as possible from local influences or contamination. Conditional sampling of model simulations to mimic these protocols may be appropriate in some cases to reduce external representation error. Many flask observation stations are located along coastlines, and the sampling protocol specifies a clean air sector from which the wind must be blowing for valid samples of background air to be taken. An example is Point Barrow, located on the Arctic coast of Alaska. Global models cannot resolve the mesoscale weather and concentration gradients in such a location, which by definition must lie at the edge of a grid cell. Spatial interpolation between the marine grid cell to the north and the land grid cell to the south would necessarily introduce just the kind of local terrestrial influence that the sampling protocol attempts to prevent. An alternative is to track these influences in the model, by simulating a tracer emitted only on land, such as ^{222}Rn [*Ramonet and Monfray*, 1996]. Monthly means can then be computed and used in response functions during only those clean air periods when the ^{222}Rn concentration was below some threshold. Several studies have assessed the impact of sampling the model output to better reflect the conditions of sample collection [*Ramonet and Monfray*, 1996; *Law*, 1996]. The impacts on estimated fluxes by inversion can be substantial when compared with results using simulated concentrations in land grid cells to represent baseline conditions, but are small compared to simply sampling an adjacent grid cell offshore [e.g., *Gurney et al.*, 2002].

3. Transport Model Error Estimation

[17] Current inversion analyses have employed a spectrum of transport models, from simple off-line advection and mixing algorithms to full-blown atmospheric GCMs. Offline models are computationally efficient, and can be driven by analyzed winds and so have some chance of capturing actual variations in transport for real periods of time. However, analyzed weather products typically do not include vertical transports by parameterized convection and other subgrid-scale processes, so they are reconstructed by the tracer model using parameterizations that are not consistent with the parent analysis. Also, analyzed weather is typically only archived four times daily, so substantial aliasing of diurnal effects on cloudiness, boundary layer mixing, and other phenomena is unavoidable. Online calculations using full climate GCMs are fully self-consistent, but can only hope to represent the transport climatology of the atmosphere and will not capture actual variations in circulation on synoptic or even interannual timescales. An ideal solution might be to carry out CO_2 inversions using online tracer transport in numerical weather forecast and analysis systems, with the full model physics, but this has not yet been attempted due to computational and logistical considerations. It is also not obvious how to constrain the model CO_2 simulations within the relatively short assimilation windows currently used with the available observations.

Table 1. Transport Model Error Effect

Source region	Model mean flux		Model standard deviation		Difference [%]
	Without model error [Gt C yr^{-1}]	With model error [Gt C yr^{-1}]	Without model error [Gt C yr^{-1}]	With model error [Gt C yr^{-1}]	
Boreal North America	0.26	0.21	0.27	0.25	−18.7
Temperate North America	−0.83	−1.11	0.42	0.35	−34.0
Tropical America	0.63	0.37	0.56	0.41	−41.9
South America	−0.16	−0.19	0.38	0.30	−13.3
North Africa	−0.17	−0.38	0.81	0.49	−124.7
South Africa	−0.32	−0.23	0.40	0.34	26.6
Boreal Asia	−0.52	−0.42	0.54	0.49	18.6
Temperate Asia	−0.62	−0.62	0.58	0.44	0.9
Tropical Asia	0.68	0.75	0.44	0.30	9.7
Australasia	0.32	0.33	0.22	0.22	5.6
Europe	−0.61	−0.64	0.35	0.33	−3.8
North Pacific	0.20	0.20	0.35	0.30	0.0
West Pacific	−0.27	−0.15	0.24	0.12	44.3
East Pacific	0.18	0.04	0.24	0.17	−77.8
South Pacific	0.27	−0.02	0.42	0.35	−106.3
Northern Ocean	0.14	0.12	0.18	0.14	−10.6
North Atlantic	−0.15	−0.11	0.30	0.20	28.7
Tropical Atlantic	−0.17	−0.14	0.15	0.12	17.0
South Atlantic	0.09	0.03	0.09	0.07	−65.7
Southern Ocean	0.41	0.53	0.25	0.24	27.5
Tropical Indian Ocean	−0.22	0.77	0.29	0.19	455.5
South Indian Ocean	0.22	0.19	0.20	0.14	−15.7

[18] Detailed comparisons of the response functions of leading transport models used in CO_2 inversions found substantial differences [*Law et al.*, 1996; *Denning et al.*, 1999b] that affect inversion results [*Gurney et al.*, 2002]. Many models are able to reproduce the major features of the observed spatial structure of well-observed tracers in the remote marine boundary layer, yet exhibit qualitative disagreement aloft and in continental interiors where observations are scarce. Many problems are related to differences in the degree of vertical mixing among models, as well as differences in resolved advection. A particularly thorny problem is the representation of diurnal and seasonal changes in ventilation and boundary layer mixing, because it is highly correlated with surface CO_2 exchange over many land regions [*Denning et al.*, 1995]. In the TransCom3 inversions, differences among models in the strength of this rectifier effect accounted for large differences in retrieved fluxes over the northern continents and errors of similar magnitude in poorly observed regions elsewhere required for global mass balance.

[19] In an attempt to estimate the transport model covariance matrix we compared forward model calculations from 16 different transport models from the TransCom3 experiment [*Gurney et al.*, 2002]. By calculating the intermodel simulated observation variability using the same surface fluxes in all the models we get an estimate of the diagonal elements of the model error covariance matrix:

$$\sigma_T^2 = \frac{1}{16}\sum_{i=1}^{16}\left(\overline{G_i(\mathbf{s},\mathbf{b})} - G_i(\mathbf{s},\mathbf{b})\right)^2 \qquad (6)$$

This estimate will be too large for some models and too small for other models, but it at least accounts for some of the transport error.

[20] To illustrate the effect of the model error we performed an inversion identical to the TransCom3 experiment, except we included the above estimated transport error. The model inversions in the original intercomparison were all performed assuming perfect transport. Table 1 shows the mean retrieved surface fluxes for the 22 regions and the standard deviations among the models for the original TransCom3 experiment ("Without Model Error") and for the case in which the estimated transport error has been included ("With Model Error").

[21] The table shows that the standard deviation between the models diminishes, because the inversions are weighted more to the prior flux estimates. The mean fluxes, however, show significant changes as shown in the last column of Table 1. It is therefore important to account for the model error in the inversions. Otherwise, incorrect transport will drive the solution to the incorrect answer.

4. Internal Representation Error Estimation

4.1. Theory

[22] As noted above the internal representation error arises when the CO_2 model inversion is performed at lower spatial and/or time resolution than the forward model calculations. In the currently standard CO_2 inversions the transport operator G is for instance calculated with a GCM on a 72×44 horizontal grid at 30 min time steps. However, the inversion itself is done on 22 basis regions using annual mean values [e.g., *Gurney et al.*, 2002]. This transformation from a relatively high resolution forward model grid to a low resolution inversion grid causes a loss of information, which translates in an extra error source.

[23] This loss of information is illustrated by defining the operator **B**:

$$\mathbf{s} = \mathbf{B}\alpha \qquad (7)$$

where α is a vector of amplitudes, **s** is the vector of surface fluxes at transport model resolution, and **B** consists of the basis functions. Equation (1) is then replaced by

$$\Phi = [\mathbf{GB}\alpha - \mathbf{d}]^T \mathbf{C}(\mathbf{d})^{-1} [\mathbf{GB}\alpha - \mathbf{d}] + [\alpha - \alpha_0]^T \mathbf{C}(\alpha_0)^{-1} [\alpha - \alpha_0] \tag{8}$$

where **GB** will be calculated directly with the transport model. These basis functions **B** can be thought of as describing flux patterns within each basis region based on prior knowledge. The basis functions also contain any prescribed information about the time dimension of the fluxes, such as diurnal, synoptic, and seasonal variations. Although these time variations are at least as important as the spatial variations, we will focus on the latter in this section. For example, if we define North America as one of the basis regions, one column of **B** would exist of zeros in all elements that represent grid boxes outside North America and ones in all elements that represent grid boxes within North America. In this example the basis function represents an average flux for North America. Or instead of setting grid boxes within North America to one, we could also add more detail in the form of a regional flux pattern. The amplitudes α, on which we perform the inversion, then define the strength of these flux patterns. It is very important to realize that if a given flux field is represented by α, we are only considering states of the form $\mathbf{B}\alpha$ as candidates for retrieved flux fields! All other possible flux fields can not be candidates for the solution. Using the example above, the inverted fluxes in North America will all have the same amplitude. To use the basis functions **B** with their amplitudes α we also need the inverse operator **B*** to transform from a general flux field **s** to α:

$$\alpha = \mathbf{B}^*\mathbf{s} \tag{9}$$

This operator is used to define the prior α vector from our priori estimate of **s**. **B*** is a pseudo inverse, which satisfies $\mathbf{B}^*\mathbf{B} = \mathbf{I}$ but not $\mathbf{BB}^* = \mathbf{I}$, where **I** is the identity matrix. This means that fine-scale structure in s is lost when we transform it to α and then back to **s**. Disaggregation after inversion to produce fine-scale maps of surface fluxes is therefore not feasible or justified. To calculate **B*** we can minimize the difference between the actual state **s** and the interpolated fit $\mathbf{B}\alpha = \mathbf{BB}^*\mathbf{s}$ in the simple least squares sense providing

$$\mathbf{B}^* = \left(\mathbf{B}^T\mathbf{B}\right)^{-1}\mathbf{B}^T \tag{10}$$

or in a weighted least squares sense providing

$$\mathbf{B}^* = \left(\mathbf{B}^T\mathbf{C}(\mathbf{s}_0)^{-1}\mathbf{B}\right)^{-1}\mathbf{B}^T\mathbf{C}(\mathbf{s}_0)^{-1} \tag{11}$$

The weighted least squares method is preferable when we have more confidence in some elements of **s** than in others. This latter formulation was also used by Kam2001.

[24] Finally, we can describe an observation vector **d** as

$$\mathbf{d} = \mathbf{GB}\alpha + \epsilon_{\mathbf{d}} + \epsilon_R \tag{12}$$

where ϵ_d is the combination of observational error and transport error, and ϵ_R is the representation error that can be calculated with

$$\begin{aligned} \epsilon_R &= \mathbf{Gs} - \mathbf{GB}\alpha \\ &= \mathbf{Gs} - \mathbf{GBB}^*\mathbf{s} \\ &= \mathbf{G}(\mathbf{I} - \mathbf{BB}^*)\mathbf{s} \end{aligned} \tag{13}$$

The prior covariance matrix has to be transformed by

$$\mathbf{C}(\alpha_0) = \mathbf{B}^*\mathbf{C}(\mathbf{s}_0)\mathbf{B}^{*T} \tag{14}$$

[25] The purpose of the operator **B** is to decrease the scale of the inversion. It is an interpolation operator. Classic inversion theory allows for this grid conversion as long as the error ϵ_R remains small [e.g., *Rodgers*, 2000]. This is important, because the operator **B** acts as a hard constraint instead of a weak constraint. A hard constraint does not allow for any error in the specification of the prior information (in this case the basis functions), while a weak constraint includes the error covariance of this prior information in the minimization process (e.g., the full prior flux estimate vector plus its error covariance matrix) [e.g., *Wunsch*, 1996]. So, instead of using the prior knowledge of flux patterns as a flexible weak constraint, the operator **B** treats this information as an inflexible hard constraint. The only flexibility left is the amplitude vector α with its corresponding prior estimate and covariance as a limited weak constraint. So, the magnitude is still flexible, but the pattern is fixed. Whenever this pattern is not the right pattern, biased inversion results will be obtained as we will illustrate in the next sections.

4.2. Two-Box Example

[26] To exemplify the deficiencies of CO_2 inversions on large regions with specified basis functions, we use the same two-box model as Kam2001 used to discuss the aggregation error. It is based on the following transport equations:

$$\begin{aligned} \frac{M}{2}\frac{dc_1}{dt} &= s1 - \frac{M}{2}\kappa(c_1 - c_2) \\ \frac{M}{2}\frac{dc_2}{dt} &= s2 - \frac{M}{2}\kappa(c_2 - c_1) \end{aligned} \tag{15}$$

where c_1 and c_2 denote the concentration in the Northern and Southern Hemispheres, respectively [cf. *Czeplak and Junge*, 1974]. The sources in the two hemispheres are denoted by s_1 and s_2, M is the mass of the atmosphere including the conversion factor from a mass mixing ratio to a volume mixing ratio, and κ is the exchange rate of air parcels between hemispheres as a fraction of the hemispheric air per time. We can describe the observations of different stations as follows:

$$\mathbf{d} = \mathbf{Gs} \tag{16}$$

where **s** represents the surface fluxes, and **G** is the transport operator (similar to the operator **J** of Kam2001). The observation vector **d** represents the change in concentration

Table 2. Simple Basis Function: Correct Prior Fluxes (**B** = [1, 1, 1, 1], $\mathbf{s}_0$ = [−3.5, −2.0, 1.0, −0.5])

	Full inversion	Uncorrected simple inversion	Corrected simple inversion
s_1 [Gt C]	−3.5	−1.6	−1.3
s_2 [Gt C]	−2.0	−1.6	−1.3
s_3 [Gt C]	1.0	−1.6	−1.3
s_4 [Gt C]	−0.5	−1.6	−1.3
$\mathbf{S}_{tot}$ [Gt C]	**−5.0**	**−6.6**	**−5.0**
$\hat{d}_1$ [ppmv]	−4.6	−3.1	−2.4
$\hat{d}_2$ [ppmv]	−4.6	−3.1	−2.4
$\hat{d}_3$ [ppmv]	−0.1	−3.1	−2.4

Table 3. Simple Basis Function: Incorrect Prior Fluxes (**B** = [1, 1, 1, 1], $\mathbf{s}_0$ = [−3.5, +2.0, 1.0, −0.5])

	Full inversion	Uncorrected simple inversion	Corrected simple inversion
s_1 [Gt C]	−5.5	−1.6	−1.2
s_2 [Gt C]	0.0	−1.6	−1.2
s_3 [Gt C]	1.0	−1.6	−1.2
s_4 [Gt C]	−0.5	−1.6	−1.2
$\mathbf{S}_{tot}$ [Gt C]	**−5.0**	**−6.5**	**−5.0**
$\hat{d}_1$ [ppmv]	−4.6	−3.1	−2.4
$\hat{d}_2$ [ppmv]	−4.6	−3.1	−2.4
$\hat{d}_3$ [ppmv]	−0.1	−3.1	−2.4

with respect to a well-mixed base state assuming constant fluxes over a period Δt. According to Kam2001 **s** represented the sum of the sources and the difference of the sources. Here, we use **s** just as the individual fluxes of the two hemispheres and **G** can be written as follows:

$$\mathbf{G} = \begin{pmatrix} \frac{\Delta t}{M} + \frac{1}{2M\kappa}\left(1 - e^{-2\kappa\Delta t}\right) & \frac{\Delta t}{M} - \frac{1}{2M\kappa}\left(1 - e^{-2\kappa\Delta t}\right) \\ \frac{\Delta t}{M} + \frac{1}{2M\kappa}\left(1 - e^{-2\kappa\Delta t}\right) & \frac{\Delta t}{M} - \frac{1}{2M\kappa}\left(1 - e^{-2\kappa\Delta t}\right) \\ \frac{\Delta t}{M} - \frac{1}{2M\kappa}\left(1 - e^{-2\kappa\Delta t}\right) & \frac{\Delta t}{M} + \frac{1}{2M\kappa}\left(1 - e^{-2\kappa\Delta t}\right) \end{pmatrix} = \begin{pmatrix} G_1 & G_2 \\ G_1 & G_2 \\ G_2 & G_1 \end{pmatrix} \quad (17)$$

in the case of 2 observations in the Northern Hemisphere and 1 observation in the Southern Hemisphere.

[27] Although the two-box examples by Kam2001 were useful to get an understanding of the problem, they did not show the impact of using basis functions when the problem is underdetermined, i.e., when there are more unknowns than observations as is the case with global inversions. To illustrate this problem we divided the individual fluxes in the two boxes in two separate fluxes (e.g., an anthropogenic and a natural flux). This provides 4 unknowns with 3 observations. The G-matrix then changes into the following 4 × 3 matrix

$$G = \begin{pmatrix} G_1 & G_1 & G_2 & G_2 \\ G_1 & G_1 & G_2 & G_2 \\ G_2 & G_2 & G_1 & G_1 \end{pmatrix} \quad (18)$$

The specified surface fluxes are set to $s_1 = -3.5$ Gt C, $s_2 = -2.0$ Gt C, $s_3 = 1.0$ Gt C, and $s_4 = -0.5$ Gt C, which provide the following observation values: $d_1 = -4.6$ ppmv, $d_2 = -4.6$ ppmv, and $d_3 = -0.1$ ppmv. In the following examples we performed three types of inversions: a full inversion on all 4 fluxes using the 3 observations, a simple inversion on the amplitude of one basis function without accounting for the possible error (see equation (12)), and a simple inversion on the amplitude of one basis function that accounts for the representation error.

[28] The first example uses a prior flux guess equal to the real surface fluxes and a basis function vector of [1, 1, 1, 1]. This means that in the simple inversions all fluxes will have the same amplitude. Results are presented in Table 2. The full model inversion retrieves exactly the right answer for the individual surface fluxes and the total flux, because the observations have no error and the prior guess is equal to the real fluxes. Also, the predicted observations $\hat{d}_1$, $\hat{d}_2$, and $\hat{d}_3$ using the inverted surface fluxes are the same as the observations. However, the simple inversion using the basis function provides the wrong answer for the total flux (−6.6) when we do not correct for the representation error by increasing the observational covariance matrix. When we do correct for the representation error the inversion is able to come up with almost the right answer for the total flux, although the individual fluxes are wrong. This result was also shown by Kam2001, although they did not use any prior constraint. It is important to note that these errors are caused by using a wrong basis function. If we would have used the correct basis function, no inversion errors would have been made.

[29] Our second example uses the simple basis function of the first example, but now has a prior flux estimate that is incorrect. The prior flux estimate for s_1, s_3, and s_4 are again equal tot the real surface fluxes, but the prior estimate of s_2 is +2.0 Gt C instead of −2.0 Gt C. The results are shown in Table 3. The full inversion is now not able to retrieve the exact values for the individual fluxes, but still gives the right answer for the total flux. The two simple inversions have basically the same answers as in the first example with some small changes due to the changed prior flux estimate, which produces a small change in the prior basis function amplitude estimate.

[30] The third example shows the most realistic situation, where the prior guess is not equal to the real fluxes (as in example 2) and where the basis function is based on this prior flux estimate (**B** = [−3.5, 2.0, 1.0, −0.5]). The result for the full inversion is the same as in example 2, as is shown in Table 4. The results of the simple inversions, however, have changed dramatically. Since there is no way

Table 4. Incorrect Basis Functions: Incorrect Prior Fluxes ($\mathbf{s}_0$ = **B** = [−3.5, +2.0, 1.0, −0.5])

	Full inversion	Uncorrected simple inversion	Corrected simple inversion
s_1 [Gt C]	−5.5	−11.1	−4.1
s_2 [Gt C]	0.0	6.4	2.3
s_3 [Gt C]	1.0	3.2	1.2
s_4 [Gt C]	−0.5	−1.6	−0.6
$\mathbf{S}_{tot}$ [Gt C]	**−5.0**	**−3.2**	**−1.2**
$\hat{d}_1$ [ppmv]	−4.6	−3.9	−1.4
$\hat{d}_2$ [ppmv]	−4.6	−3.9	−1.4
$\hat{d}_3$ [ppmv]	−0.1	0.9	0.3

Table 5. Estimated Flux Differences Caused by the Internal Representation Error Effect

Source region	Posterior [Gt C yr^{-1}]	CandN experiment		Flat experiment		SiB2 experiment	
		Gt C yr^{-1}	%	Gt C yr^{-1}	%	Gt C yr^{-1}	%
Boreal North America	0.57	0.04	14.6	0.26	84.5	−0.28	−91.0
Temperate North America	0.57	−0.03	−2.0	−0.19	−12.0	0.43	27.8
Tropical America	1.09	0.10	23.3	0.10	22.9	0.47	112.7
South America	0.98	−0.02	−13.2	−0.03	−18.9	0.35	201.3
North Africa	1.08	0.14	49.9	0.12	43.0	−0.41	−143.2
South Africa	0.80	0.00	20.8	0.03	158.8	0.10	446.8
Boreal Asia	0.52	−0.32	−33.6	0.01	1.0	0.63	67.1
Temperate Asia	0.79	−0.06	−4.6	−0.37	−29.5	−0.20	−15.6
Tropical Asia	0.73	−0.05	−6.6	0.04	5.3	−0.31	−42.1
Australasia	0.33	−0.08	−135.2	−0.09	−148.4	0.04	58.4
Europe	0.50	0.31	47.0	0.15	22.7	0.13	19.4
North Pacific	0.28	0.07	28.9	0.04	18.4	−0.11	−43.5
West Pacific	0.30	−0.10	−56.5	−0.02	−11.6	0.17	99.2
East Pacific	0.45	0.01	4.3	0.02	7.2	0.04	17.0
South Pacific	0.48	0.03	26.1	0.06	43.6	−0.32	−251.5
Northern Ocean	0.15	−0.10	−142.6	−0.08	−109.9	−0.43	−621.9
North Atlantic	0.35	0.04	16.9	0.06	24.9	−0.11	−41.8
Tropical Atlantic	0.30	0.02	5.4	−0.07	−22.5	0.01	5.0
South Atlantic	0.44	−0.01	−16.4	−0.00	−12.8	0.01	38.3
Southern Ocean	0.29	−0.01	−10.3	−0.02	−15.0	−0.12	−92.1
Tropical Indian Ocean	0.50	−0.02	−3.5	−0.02	−4.1	−0.17	−31.1
South Indian Ocean	0.37	0.01	24.4	−0.01	−14.1	0.06	113.9

in these simple inversions to change the assumed pattern (in contrast to the full inversion, in which the individual fluxes can be changed based on the available information from the observations), the inversion algorithm is not able get a good match with the observations. Accounting for the representation error seems to make things worse, since it drives the solution more to the wrong prior estimate for the basis function amplitude. However, the posterior error estimate (not shown) is increased such that the solution falls within the error estimate, in contrast to the uncorrected case. This last example clearly illustrates the difference between a hard and a weak constraint. The weak constraint has flexibility defined by the prior error covariance that allows for using the information from the observations wherever possible. The prior flux estimate can therefore be adjusted to provide the answer that is closest to the real answer considering the prior covariances and observation covariances. The hard constraint, however, is not flexible at all and will drive the solution to an incorrect answer when the prior flux estimate (on which the basis function is based) has errors in it, as is usually the case. The assumed pattern can only be moved up or down defined by the retrieved amplitude and has no flexibility to adjust the individual fluxes to get a better match with the observations. The inclusion of the representation error in the inversion will only assure that we do not over interpret our results, it does not provide a better solution.

4.3. Global Inversions

[31] Although the simple two-box model is useful for understanding the basic problems with the use of basis functions, it is important to make the link to the full GCM inversions. In the recent TransCom3 model comparisons [*Gurney et al.*, 2002], CO_2 flux inversions of several models were compared. Annual mean CO_2 concentrations from 77 flask stations were inverted with the models to retrieve the amplitudes of the flux patterns of 22 basis regions (see Figure 1), the amplitudes of fossil fuel, neutral biosphere, and oceanic carbon exchange fluxes, and an offset value. Each amplitude value has a prior guess with a matching prior error estimate. The prior errors of the fossil fuel, neutral biosphere, and oceanic carbon exchange flux amplitudes were set to very small values. This way, these flux amplitudes cannot be changed in the inversion and therefore are called presubtracted flux fields. The prior errors of the basis region amplitudes are all set to large values, which leaves the inversion free to change the prior estimates. All models used the same set of basis regions with basis functions specified from prior knowledge about natural flux patterns. The analogy with the two-box model is that the prior information about the flux patterns within each basis region is specified as a hard constraint through the use of the basis functions. This allows no flexibility in the retrieved flux patterns and therefore will produce incorrect results in case the specified flux patterns are not correct. Another set of hard constraints are the presubtracted flux fields. Since the prior errors are almost zero, any error in our estimate of these fluxes and their spatial and temporal structure cannot be adjusted and will therefore produce errors in the retrieval of the fluxes for the 22 basis regions.

[32] To illustrate the problem of incorrect specification of spatial structure within the basis regions, we performed the annual mean TransCom3 inversion using response functions of the Colorado State University (CSU) GCM [e.g., *Randall et al.*, 1996; *Fowler and Randall*, 1999; *Eitzen and Randall*, 1999] produced from surface fluxes using the original TransCom3 "footprints." All three experiments used the same set of regional fluxes at the 22-region resolution of the inversion, but subregional distributions were varied to produce basis function error. Our control experiment distributed the fluxes according to the annual net primary production simulated by the CASA ecosystem model [*Randerson et al.*, 1997], exactly as in the original TransCom3 experiment. Pseudodata from this experiment can be

inverted to retrieve fluxes for each region. This control inversion eliminates any transport error and representation error. Therefore, the inverted fluxes will be defined by the simulated observations and the prior fluxes using the specified observational errors and the prior flux errors as weights. Two other experiments (CandN and Flat) used different subregional distributions of the surface fluxes to simulate observations and are defined in Appendix A. Our setup is similar to inverting one set of observations using three sets of basis functions, but saves the calculation of three different sets of response functions. Differences between the CandN and Flat inversions and the control inversion are shown in Table 5 both in Gt C yr^{-1} and % as CandN experiment and Flat experiment.

[33] As can be expected, the largest differences are found over land, where the flux footprints have the largest differences among the three experiments. For instance, the inverted fluxes for Boreal North America, Europe, Temperate Asia, and Northern Africa change substantially when using different basis functions for the inversion. An example of the often unpredictable nature of these errors is Boreal Asia. While the spatial pattern difference between the CASA footprint of the control inversion and the flat footprint of the Flat inversion is much larger than the difference between the CASA footprint of the control inversion and the footprint of the CandN inversion, the difference between the CASA fluxes and the flat fluxes are small and the difference between the CASA fluxes and the CandN fluxes are large. Temperate North America shows comparable retrieved fluxes using the CASA footprint and the CandN footprint, but a quite different retrieved flux using the Flat footprint. Figure A1 shows that the Flat footprint is not a good approximation of the CASA or CandN footprints, while the latter two are reasonably similar. However, relatively larger differences in the retrieved fluxes are observed downwind of the North American landmass over the Northern Ocean. Apparently, differences between the CASA and the CandN footprint have a larger effect here. When we try to account for the representation error using equation (12), differences from the true flux do not become smaller. The solutions are driven closer to the prior estimates, because the values of $\mathbf{C}(\mathbf{d})$ are increased (not shown). However, this does not generate better solutions to the inverse problem. Although differences between the three inversions are noticeable, they generally fall within the posterior error estimates (second column in Table 5). They could however become more significant when more observations are used in the inversion calculations and/or when the transport model errors are reduced. The errors shown in Table 5 will only be reduced when the hard constraint setup is replaced by a weak constraint setup.

[34] The use of presubtracted flux patterns can even lead to larger errors in the inverted fluxes as will be shown below. Although we have a reasonable knowledge about these prescribed fluxes, our knowledge is not exact. For instance, the total fossil fuel emission per country is known accurately, but the distribution in space and time per country is less well known. Currently, the fossil fuel emission rates within a country are distributed according to population numbers. However, power plants and cement plants are not always located in high population areas. Also, seasonal, daily, and diurnal emissions are not documented in detail. Here, we consider the effect of uncertainties in the neutral biosphere fluxes on the inversions. The description of the neutral biosphere fluxes used in TransCom3 is based on the CASA model [*Randerson et al.*, 1997]. Although this is a reasonable estimate of these fluxes, it is by no means the only estimate possible. We used an estimate based on the SiB2 model [*Denning et al.*, 1996] as an alternative to the CASA estimate. Although both estimates have a zero annual mean flux, they differ significantly both in time and space.

[35] Figure 2 shows annual mean concentration fields using the CASA fluxes and the SiB2 fluxes, respectively. Large differences are visible, which are mainly caused by the rectifier effect acting on flux distributions that are different in amplitude and phase. This means that although the annual mean flux of both flux distributions is zero, large differences in the annual mean CO_2 concentrations are produced by the interaction of the transport with flux distributions that differ in time and space. The SiB2 experiment columns in Table 5 show the results of the inversion with the SiB2 fluxes used for the prescribed neutral biosphere fluxes relative to the control inversion using the CASA fluxes. Large differences in the inverted fluxes are found. Apparently, two equally valid estimates of the neutral biosphere fluxes can produce two very different answers to the inversion problem. Again, this is caused by imposing a hard constraint that does not allow any changes in the assumed prior flux estimate. Also noteworthy is that the errors of the SiB2 experiment are larger than the two other experiments. Because the specification of the neutral biosphere fluxes have a much larger impact on the simulated observations than the relatively small fluxes of the 22 individual basis regions, any errors in the prior assumptions will have a larger impact on the inversion results.

5. Conclusions

[36] In atmospheric CO_2 inversions it is important to account for all relevant sources of error. In the general inversion equation (equation (3)) these errors are split into two categories, the prior errors defining our confidence in the prior estimate of the surface fluxes, and the errors representing the expected difference between the model simulations and the observations. The latter category of errors should contain several different sources of error, although quite often only the observation error is taken into account. This leads in the best case to misleading discussions about the value of the observations and in the worst case to incorrect inversion results.

[37] Not accounting for certain error sources can be defined as applying hard constraints to the inversion problem. A hard constraint uses prior information relevant to the inversion problem and applies it without any flexibility in case the prior assumptions are wrong. In most cases this will lead to incorrect inversion results. On the other hand, a weak constraint also applies prior information to the inversion problem, but allows flexibility to these assumptions within the margins of the defined prior error covariance. If estimated correctly, these prior assumptions and especially these prior covariance matrices will constrain the problem correctly. It is important to note here that using prior information with very small prior error estimates in cases where this is not justified basically acts as a hard constraint as well.

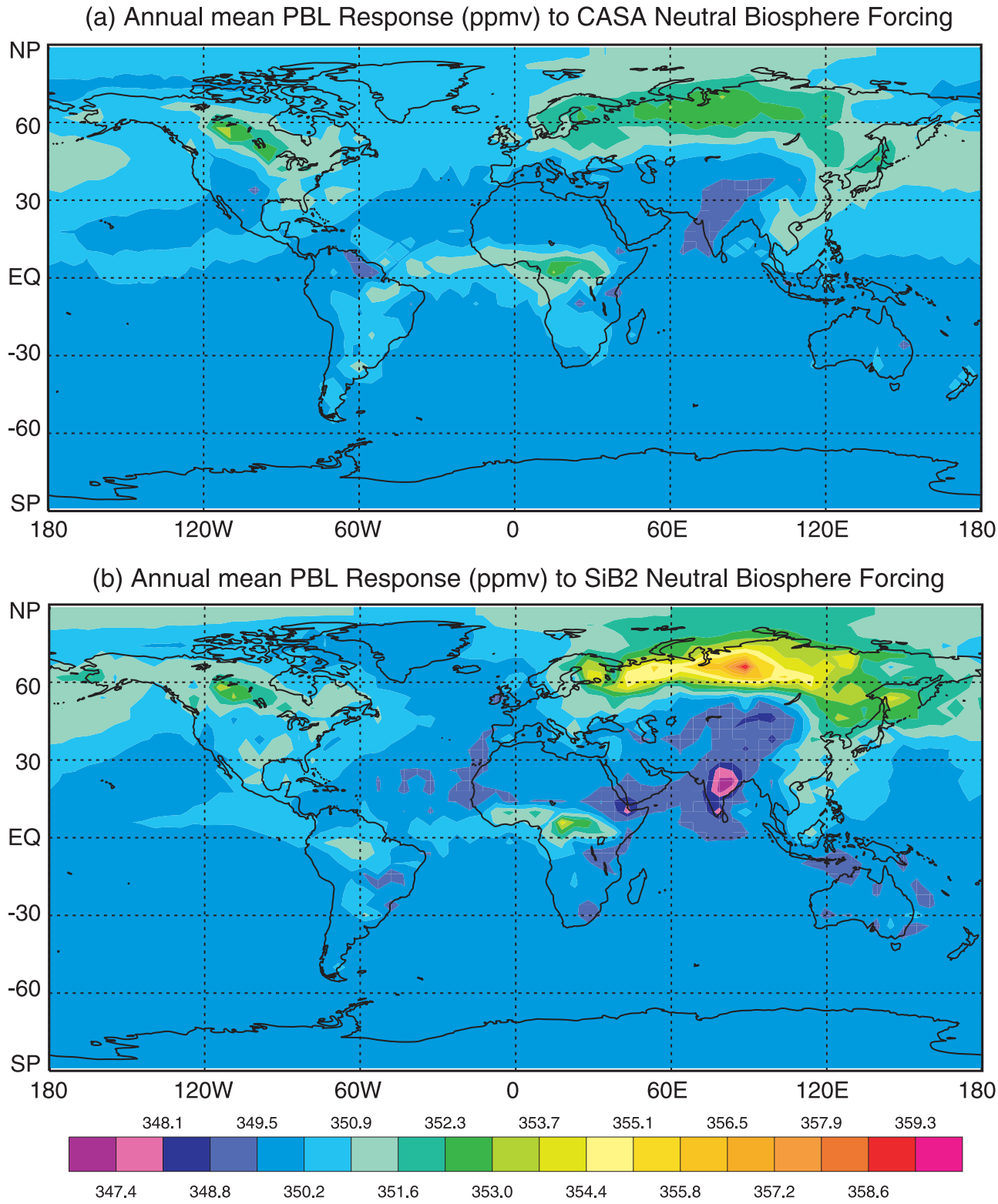

Figure 2. Annual mean response of concentration in the planetary boundary layer to purely seasonal forcing by balanced terrestrial biota as simulated by the CSU GCM. (a) Response to fluxes from CASA model used in TransCom3. (b) Response to SiB2 model fluxes.

[38] We discussed in more detail two sources of error that are often applied as hard constraints, the model transport error and the internal representation error. When the model transport error is not taken into account, we assume a perfect relation between CO_2 concentration observations and surface fluxes. This will give too much weight to the observations in the inversion. Proper accounting for the model transport error will give proper weights to the observations depending on how well our transport model is able to model regional and large-scale transport. So, even perfect observations will have to be weighted properly depending on how well our transport model is able to model the relationship between these observations and the surface fluxes.

[39] The internal representation error is harder to deal with, because it cannot be completely accounted for. Specifying fixed footprints in large regions or seasonal or diurnal patterns of fluxes will limit the possible solutions to the inversion problem to exactly those assumed patterns. Only the amplitudes of these footprints can be changed during the inversion. If the assumed flux pattern is incorrect, the solution within each basis region will be incorrect, which can lead to incorrect aggregated fluxes for each basis region. Methods to account for this representation error will avoid overinterpretation of the results, but will not necessarily provide a better solution. Also the specification of a prior constraint with very small prior errors, as was done in the TransCom3 experiment with the neutral biosphere and the fossil fuel fluxes, will often lead to incorrect results if these small prior errors are not justified.

[40] Most optimal would be to invert on the native transport model grid and time step with the prior knowledge of the fluxes fully specified as a weak constraint taking the spatial and temporal correlations fully into account. This allows for an optimal use of the information contained in the observations. If the observations contain little information about the fluxes in a certain area, the retrieved fluxes will basically reflect the prior estimate. If the observations do contain information about the fluxes in a certain region, the fluxes in that region will be adjusted to match the simulated concentrations with the observations. Proper inversion statistics (e.g., averaging kernels [*Rodgers*, 2000]) will show where we retrieve the prior estimates back and where we will retrieve new information about the fluxes. This also allows for a more continuous improvement of our flux estimates when more and better observations become available. However, with the current transport models this is hard to accomplish, especially since most of these models use simple perturbation methods to estimate the response functions instead of using an adjoint model as used by *Kaminski et al.* [1999]. The calculation of the response functions for every grid box and time step would therefore be a very cumbersome task. It is important, however, to be aware of the possible representation errors and to make an effort to minimize these errors. Downscaling the inversion problem by using large regions and assumed temporal patterns is too rigid and leads to unavoidable bias in the retrieved fluxes. Especially, with increased flask measurement programs and the next generation satellites providing many more observations [*Engelen et al.*, 2001] modelers should make an effort to make full use of these observations and avoid any hard constraints on the problem.

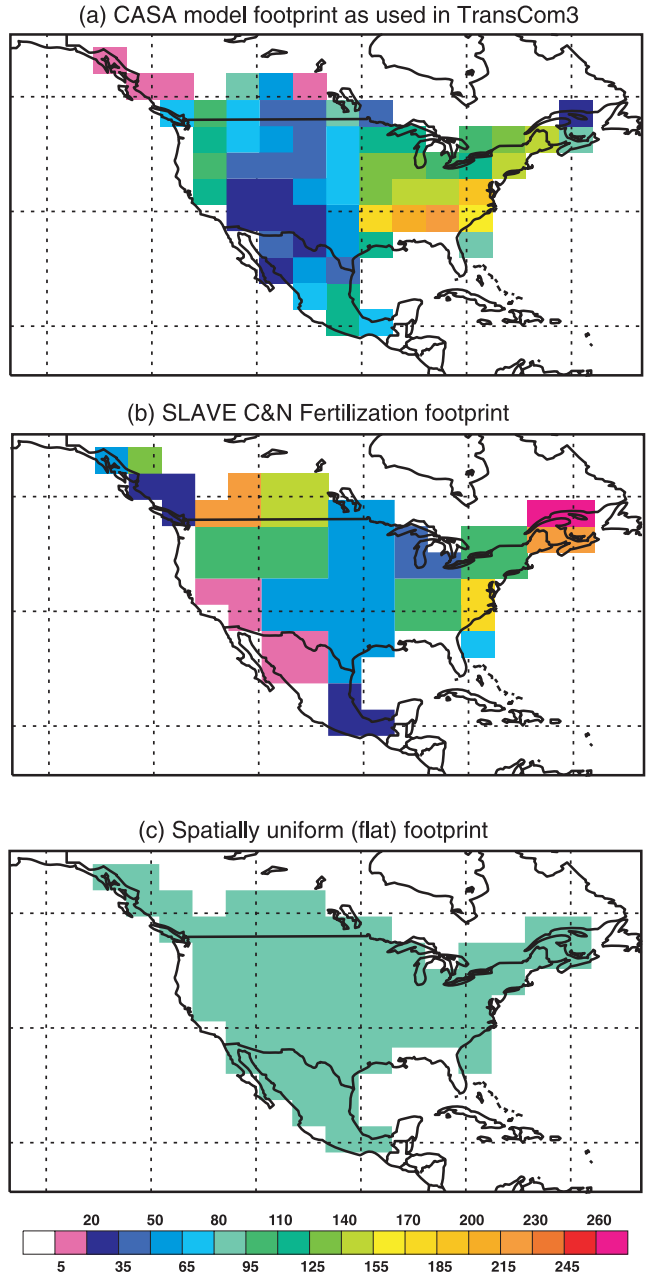

Figure A1. Subregional spatial structure of surface fluxes (g C m^{-2} yr^{-1}) from Temperate North America as simulated in three forward simulations with the CSU GCM. Annual global integral of each field is exactly 1 Gt C yr^{-1}, scaled by inversion to optimize agreement with observed CO_2.

[41] Finally, we would like to point out the use of full data assimilation systems as are being used in numerical weather prediction. These would allow a better use of the current and future observations by using observations when and where they are available to constrain the forward model run. This way we could even constrain biological surface flux processes (if modeled in the data assimilation model) with such observation as satellite surface vegetation maps or ocean surface chlorophyll concentrations. For this to work, however, it is important to have enough (near) real-time observational data that can adequately constrain the forward

model CO_2 simulations. Although this kind of full data assimilation to invert surface CO_2 fluxes may still be years down the road, we think it is important to head in that direction and start thinking how to make best use of the available observations.

Appendix A

[42] The experiments described in section 4.3 are chosen to illustrate the effect of prescribed basis functions on the inversion of surface fluxes. The CandN experiment uses subregional distributions reflecting the effects of net sinks due to CO_2 and nitrogen fertilization simulated by the SLAVE model [*Denning et al.*, 1999a]. The Flat experiment uses spatially homogeneous (flat) distributions of surface fluxes within each region. The spatial distributions of surface fluxes in the control and the CandN experiments are qualitatively similar, representing two quite plausible distributions based on prior knowledge. The differences in the inversions produced by these different footprints are probably quite reasonable estimates of the magnitude of errors in actual inversions arising from incorrect spatial distribution of surface fluxes in basis regions of this size. The distribution used in the Flat experiment is not reasonable based on prior knowledge: for example the Sahara and the Congo Basin are assumed to be equally responsible for any source or sink in northern Africa. The inversion errors produced by these pseudodata represent an extreme case and bracket the magnitude of errors in retrieved fluxes arising from internal representation error. Some people might argue it is more appropriate to use flat basis functions because they feel we are cheating by using prior knowledge to specify spatial patterns within basis regions. We should point out that unadjustable spatial structure is a hard constraint, whether it is flat or reasonable. And since flat is very unlikely at these spatial scales, such an approach is likely to produce worse bias, not less, than we get using prior knowledge to specify these spatial structures. It should also be pointed out here that in our setup with a number of presubtracted flux patterns (e.g., neutral biosphere and fossil fuel) on which the inverted basis region fluxes are adjustments, the effect of the chosen basis functions is smaller than when we would invert without presubtracted flux patterns. Figure A1 shows the three different footprints for temperate North America.

[43] **Acknowledgments.** The work described in this paper was supported by NASA contract NCC5-621 and NOAA contract NA17RJ1228. The TransCom3 experiment was made possible through support from the National Science Foundation (OCE-9900310), the National Oceanic and Atmospheric Administration (NA67RJ0152, Amend 30), and the International Geosphere Biosphere Program/Global Analysis, Interpretation, and Modeling Project. We thank Ian Enting and another anonymous reviewer for their substantive and constructive comments.

References

Andres, R. J., G. Marland, I. Fung, and E. Matthews, A 1×1 distribution of carbon dioxide emissions from fossil fuel consumption and cement manufacture, 1950–1990, *Glob. Biogeochem. Cycles*, *10*, 419–430, 1996.

Baker, D. F., Sources and sinks of atmospheric CO_2 estimated from batch least-squares inversions of CO_2 concentration measurements, Ph.D. thesis, Princeton Univ., Princeton, N. J., 2001.

Bousquet, P., P. Peylin, P. Ciais, C. Le Quéré, P. Friedlingstein, and P. P. Tans, Regional changes in carbon dioxide fluxes of land and ocean since 1980, *Science*, *290*, 1342–1346, 2000.

Czeplak, G., and C. Junge, Studies of interhemispheric exchange in the troposphere by a diffusion model, *Adv. Geophys.*, *18B*, 57–72, 1974.

Denning, A. S., I. Y. Fung, and D. Randall, Latitudinal gradient of atmospheric CO_2 due to seasonal exchange with land biota, *Nature*, *376*, 240–243, 1995.

Denning, A. S., J. G. Collatz, C. Zhang, D. A. Randall, J. A. Berry, P. J. Sellers, G. D. Colello, and D. A. Dazlich, Simulations of terrestrial carbon metabolism and atmospheric CO_2 in a general circulation model, 1, Surface carbon fluxes, *Tellus, Ser. B*, *48*, 521–542, 1996.

Denning, A. S., T. Takahashi, and P. Friedlingstein, Can a strong atmospheric CO_2 rectifier effect be reconciled with a "reasonable" carbon budget?, *Tellus, Ser. B*, *51*, 249–253, 1999a.

Denning, A. S., et al., Three-dimensional transport and concentration of SF6: A model intercomparison study (TransCom 2), *Tellus, Ser. B*, *51*, 266–297, 1999b.

Denning, A. S., K. R. Gurney, R. J. Engelen, G. L. Stephens, D. O'Brien, P. J. Rayner, and TransCom Modelers, Potential constraints on the global carbon budget using satellite retrievals of atmospheric CO_2, in *Extended Abstracts of the Sixth International Carbon Dioxide Conference, Sendai, Japan*, 2001.

Eitzen, Z. A., and D. A. Randall, Sensitivity of the simulated Asian summer monsoon to parameterized physical processes, *J. Geophys. Res.*, *104*, 12,177–12,191, 1999.

Engelen, R. J., A. S. Denning, K. R. Gurney, and G. L. Stephens, Global observations of the carbon budget, 1, Expected satellite capabilities for emission spectroscopy in the EOS and NPOESS eras, *J. Geophys. Res.*, *106*, 20,055–20,068, 2001.

Enting, I. G., *Inverse Problems in Atmospheric Constituent Transport*, Cambridge Univ. Press, New York, 2002.

Enting, I. G., C. M. Trudinger, and R. J. Francey, A synthesis inversion of the concentration and d13C of atmospheric CO_2, *Tellus, Ser. B*, *47*, 35–52, 1995.

Fan, S., M. Gloor, J. Mahlman, S. Pacala, J. Sarmiento, T. Takahashi, and P. Tans, A large terrestrial carbon sink in North America implied by atmospheric data and oceanic carbon dioxide data and models, *Science*, *282*, 442–446, 1998.

Fowler, L. D., and D. A. Randall, Simulation of upper tropospheric clouds with the CSU general circulation model, *J. Geophys. Res.*, *104*, 6101–6121, 1999.

Gurney, K. R., R. M. Law, P. J. Rayner, and A. S. Denning, TransCom 3 experimental protocol, *Tech. Rep. 707*, Dept. of Atmos. Sci., Colo. State Univ., Fort Collins, Colo., 2000.

Gurney, K. R., et al., Towards robust regional estimates of CO_2 sources and sinks using atmospheric transport models, *Nature*, *415*, 626–630, 2002.

Kaminski, T., M. Heimann, and R. Giering, A coarse grid three-dimensional global inverse model of the atmospheric transport, 1, Adjoint model and Jacobian matrix, *J. Geophys. Res.*, *104*, 18,535–18,553, 1999.

Kaminski, T., P. J. Rayner, M. Heimann, and I. G. Enting, On aggregation errors in atmospheric transport inversions, *J. Geophys. Res.*, *106*, 4703–4715, 2001.

Law, R. M., The selection of model-generated CO_2 data: A case study with seasonal biospheric sources, *Tellus*, *48B*, 474–486, 1996.

Law, R. M., et al., Variations in modeled atmospheric transport of carbon dioxide and the consequences for CO_2 inversions, *Glob. Biogeochem. Cycles*, *10*, 783–796, 1996.

Masarie, K. A., et al., NOAA/CSIRO flask air intercomparison experiment: A strategy for directly assessing consistency among atmospheric measurements made by independent laboratories, *J. Geophys. Res.*, *106*, 20,445–20,464, 2001.

Ramonet, M., and P. Monfray, CO_2 baseline concept in 3-D atmospheric transport models, *Tellus*, *48B*, 502–520, 1996.

Randall, D. A., et al., A revised land-surface parameterization (SiB2) for atmospheric GCMs, part 3, The greening of the CSU general circulation model, *J. Clim.*, *9*, 738–763, 1996.

Randerson, J. T., M. V. Thompson, T. J. Conway, I. Y. Fung, and C. B. Field, The contribution of terrestrial sources and sinks to trends in the seasonal cycle of atmospheric carbon dioxide, *Glob. Biogeochem. Cycles*, *11*, 535–560, 1997.

Rayner, P. J., I. G. Enting, R. J. Francey, and R. Langenfelds, Reconstructing the recent carbon cycle from atmospheric CO_2, d13C, and O_2/N_2 observations, *Tellus, Ser. B*, *51*, 213–232, 1999.

Rodgers, C. D., *Inverse Methods for Atmospheric Sounding: Theory and Practice*, World Sci., River Edge, N. J., 2000.

Takahashi, T., R. H. Wanninkhof, R. A. Feely, R. F. Weiss, D. W. C. N. Bates, J. Olafsson, C. Sabine, and S. C. Sutherland, Net sea–air CO_2 flux over the global oceans: An improved estimate based on the sea–air pCO_2 difference, in *Proceedings of the 2nd International Symposium on CO_2 in the Oceans*, Natl. Inst. of Environ. Stud., Tsukuba, Japan, 1999.

Tans, P. P., I. Y. Fung, and T. Takahashi, Observational constraints on the global atmospheric CO_2 budget, *Science*, *247*, 1431–1438, 1990.

Tarantola, A., *Inverse Problem Theory: Methods for Data Fitting and Model Parameter Estimation*, Elsevier Sci., New York, 1987.

World Meteorological Organization (WMO), Report of the eighth WMO meeting of experts on carbon dioxide concentration and isotopic measurement techniques, *Rep. 121*, Global Atmos. Watch, Geneva, 1995.

World Meteorological Organization (WMO), Report of the ninth WMO meeting of experts on carbon dioxide concentration and related trace measurement techniques, *Rep. 132*, Global Atmos. Watch, Geneva, 1999.

Wunsch, C., *The Ocean Circulation Inverse Problem*, Cambridge Univ. Press, New York, 1996.

A. S. Denning and K. R. Gurney, Department of Atmospheric Science, Colorado State University, Fort Collins, CO, USA.

R. J. Engelen, European Centre for Medium-Range Weather Forecasts, Shinfield Park, Reading RG2 9AX, UK. (richard.engelen@ecmwf.int)